Structural basis for potassium transport in prokaryotes by KdpFABC

Marie E. Sweet[a], Casper Larsen[b], Xihui Zhang[a], Michael Schlame[c,d], Bjørn P. Pedersen[b,1], and David L. Stokes[a,d,1]

[a]Skirball Institute of Biomolecular Medicine, Department of Cell Biology, New York University Grossman School of Medicine, New York, NY 10016; [b]Department of Molecular Biology and Genetics, Aarhus University, 8000 Aarhus C, Denmark; [c]Department of Anesthesiology, New York University Grossman School of Medicine, New York, NY 10016; and [d]Department of Cell Biology, New York University Grossman School of Medicine, New York, NY 10016

Edited by Yifan Cheng, University of California, San Francisco, CA, and approved June 14, 2021 (received for review March 17, 2021)

KdpFABC is an oligomeric K^+ transport complex in prokaryotes that maintains ionic homeostasis under stress conditions. The complex comprises a channel-like subunit (KdpA) from the superfamily of K^+ transporters and a pump-like subunit (KdpB) from the superfamily of P-type ATPases. Recent structural work has defined the architecture and generated contradictory hypotheses for the transport mechanism. Here, we use substrate analogs to stabilize four key intermediates in the reaction cycle and determine the corresponding structures by cryogenic electron microscopy. We find that KdpB undergoes conformational changes consistent with other representatives from the P-type superfamily, whereas KdpA, KdpC, and KdpF remain static. We observe a series of spherical densities that we assign as K^+ or water and which define a pathway for K^+ transport. This pathway runs through an intramembrane tunnel in KdpA and delivers ions to sites in the membrane domain of KdpB. Our structures suggest a mechanism where ATP hydrolysis is coupled to K^+ transfer between alternative sites in KdpB, ultimately reaching a low-affinity site where a water-filled pathway allows release of K^+ to the cytoplasm.

membrane transport | P-type ATPase | energy coupling | stress response

KdpFABC is an ATP-dependent K^+ pump in prokaryotes, essential for osmoregulation in K^+-deficient environments. Expression of kdpFABC is induced when external K^+ concentrations fall into the micromolar range, where constitutive K^+-uptake systems, Trk and Kup, can no longer maintain intracellular K^+ levels. Under these conditions, a high-affinity active transport system is required to maintain internal concentrations of K^+, essential for regulating pH, membrane potential, and the turgor pressure that drives cell growth and division (1). As a molecular machine, the oligomeric KdpFABC complex represents a fascinating hybrid that couples a channel-like subunit (KdpA)—related to the superfamily of K^+ transporters (SKT)—with a pump-like subunit (KdpB)—belonging to the superfamily of P-type ATPases (2). Early studies established a role for KdpA in the selectivity and transport of K^+ (3). Furthermore, analysis of KdpA sequence and topology established the existence of four approximate repeats of the "MPM" fold that characterizes K^+ channels and a close resemblance to bacterial potassium channels TrkH and KtrB (4). KdpB, on the other hand, harnesses the energy of ATP to drive transport of K^+ against a concentration gradient. KdpB was shown to employ the Post–Albers reaction scheme (5) that features two main conformational states, E1 and E2, and an aspartyl phosphate intermediate (Fig. 1*A*). However, mechanisms for coupling between these two subunits have remained elusive, as has the specific transport pathway of K^+ through the complex (6).

Recent structural studies have generated renewed interest in KdpFABC and have led to new and conflicting ideas about its transport process. The first structure was determined by X-ray crystallography, defining the architecture of the complex (7). This structure revealed a spherical density modeled as water bound at the unwound part of the M4 transmembrane helix of KdpB (*SI Appendix*, Fig. S1*A*). This site, here denoted Bx, is conserved among P-type ATPases and plays a key role in binding and transporting their respective substrates. Structures of the well-studied sarco(endo) plasmic reticulum Ca2+-ATPase (SERCA) revealed ions at two sites, dubbed site Ca(I) and site Ca(II), the latter of which is congruent with the Bx site in KdpB. Structures of Na,K-ATPase show a similar ion binding pattern, with a third Na^+ ion also accommodated near these two conserved sites. In KdpA, a K^+ ion was bound within the selectivity filter (SF) and, like TrkH and KtrB, the third MPM repeat featured a kinked helix ($D3M_2$ in *SI Appendix*, Fig. S1*A*) with a loop that blocks this ion from traveling across the membrane. This loop was suggested to function as a gate that would move aside to open a pore for transport. In addition, a 40-Å–long tunnel was seen encapsulated within the membrane domain of KdpFABC. This intramembrane tunnel connects the SF in KdpA with the Bx site in KdpB, leading to a proposal for energy coupling based on a Grothuss mechanism for charge transfer between these sites. According to this mechanism, the tunnel is filled with water molecules acting as a water wire to shuttle protons between the subunits. K^+ binding to the SF would initiate proton hopping through the tunnel. Arrival of this charge at the Bx site would stimulate the cycle of ATP hydrolysis, as documented in other P-type ATPases. A salt-bridge network connecting cytoplasmic loops of KdpA and KdpB would then tug on the kinked $D3M_2$ helix in KdpA, thus displacing the gating loop and allowing K^+ to transit the membrane.

Two additional structures of KdpFABC were subsequently determined by cryogenic electron microscopy (cryo-EM), revealing

Significance

Potassium is the major intracellular cation in all kingdoms of life. In bacteria, potassium is used to maintain membrane potential, pH, and to provide turgor pressure for cell growth and division. When external potassium levels are low, an ATP-dependent pump called KdpFABC is essential to maintain intracellular potassium levels. This protein complex comprises a subunit descending from potassium channels and another from P-type ATPases. We used cryogenic electron microscopy to investigate this unique partnership and to address mechanisms of energy coupling and transport. We present structures corresponding to all major reaction intermediates and map distinct densities along the proposed transport pathway. Based on this data, we describe a mechanism that is unique amongst known membrane transporters.

Author contributions: B.P.P. and D.L.S. designed research; M.E.S., C.L., X.Z., M.S., B.P.P., and D.L.S. performed research; M.E.S., C.L., X.Z., M.S., B.P.P., and D.L.S. analyzed data; and M.E.S., C.L., B.P.P., and D.L.S. wrote the paper.

The authors declare no competing interest.

This article is a PNAS Direct Submission.

Published under the PNAS license.

[1]To whom correspondence may be addressed. Email: stokes@nyu.edu or bpp@mbg.au.dk.

This article contains supporting information online at https://www.pnas.org/lookup/suppl/doi:10.1073/pnas.2105195118/-/DCSupplemental.

Published July 16, 2021.

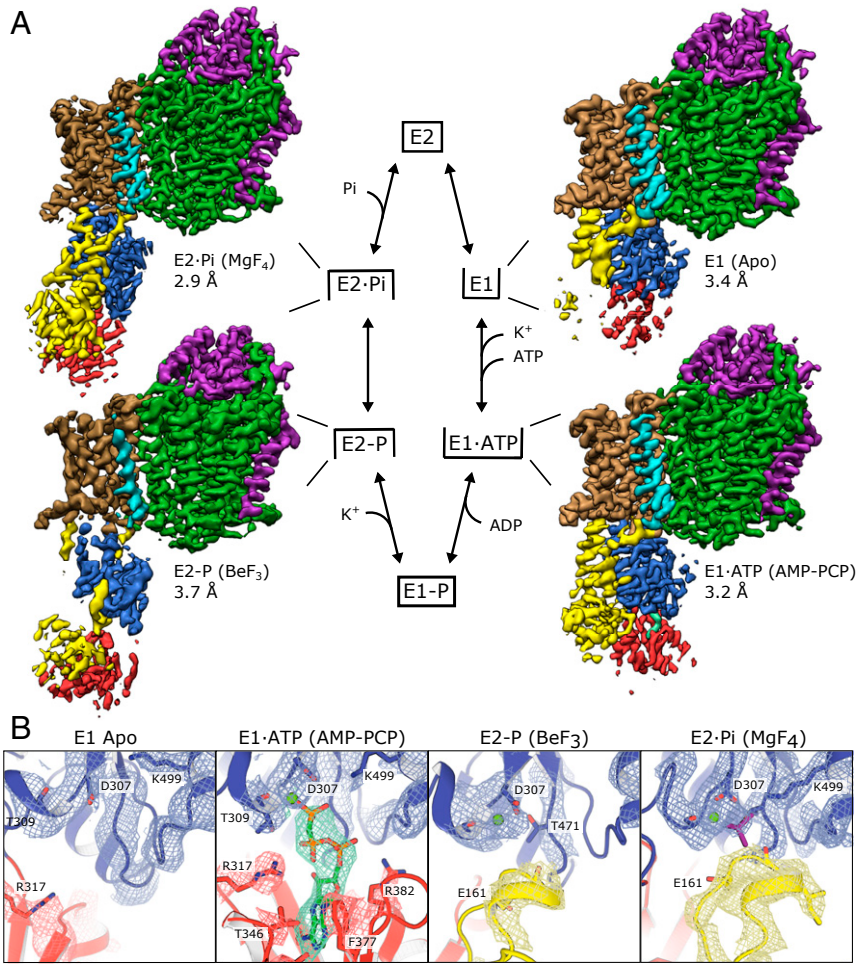

Fig. 1. Overview of cryo-EM structures. (*A*) Cryo-EM density maps of KdpFABC in four unique conformational states, corresponding to intermediates in the Post–Albers reaction cycle. KdpA is green; KdpB is brown, blue, yellow, and red; KdpC is purple; and KdpF is cyan. (*B*) Close-up of catalytic sites in which density is clearly visible for AMP-PCP and MgF_4; lower resolution of the E2-P map makes explicit placement of BeF_3 ambiguous. Mg^{2+} ions are green, and protein domains are colored as in *A*.

two additional conformations (8). Whereas the crystal structure appeared to represent an inhibited conformation due to the influence of serine phosphorylation (9), these cryo-EM structures were compatible with E1 and E2 states. The intramembrane tunnel was intact in the E1 state but was interrupted in the E2 state due to conformational changes in KdpB. These observations led to the proposal of an alternative mechanism in which K^+ ions move through the tunnel, from the SF of KdpA to the Bx site of KdpB, where they are released to the cytoplasm at the appropriate step in the reaction cycle. The other two subunits, KdpC and KdpF, were also observed in all of these structures. KdpF consists of a single transmembrane helix at the interface of KdpA and KdpB, possibly serving to stabilize the complex. KdpC has a unique periplasmic domain anchored by a single TM helix; the location at the entrance to the SF suggested that this domain might act as a periplasmic filter or gate, though evidence for this role is currently lacking.

To shed more light on the coupling between KdpA and KdpB and to resolve the role of the intramembrane tunnel, we determined structures of the KdpFABC complex in all of the major enzymatic states. We used inhibitors to trap the complex in various discrete states, in the presence of either K^+ or Na^+, and imaged these samples by cryo-EM. In this way, we produced 14 independent density maps at resolutions between 2.9 and 3.7 Å; four of these were selected to represent the primary intermediates from the reaction cycle. These resulting structures display significant conformational changes in KdpB as well as nonprotein spherical densities within the SF of KdpA, within the intramembrane tunnel, and in KdpB near the Bx site. In contrast, KdpA is static suggesting that it serves simply to select K^+ ions from the periplasm and shuttle them to transport sites in KdpB. By providing high-resolution detail to structural changes in these sites during the reaction cycle, we provide evidence and a comprehensive model for the transport mechanism in which K^+ from the periplasm enters the SF of KdpA, moves through the tunnel to the Bx site, and is released to the cytoplasm by KdpB.

Results

Cryo-EM Structures Reveal Conformational Changes of KdpFABC. For this work, we introduced the Q116R mutation into KdpA and the S162A mutation into KdpB. In previous work (9), we showed that this construct is fully functional and offers practical advantages for comparative study of reaction intermediates. Whereas the wild-type protein features very high (micromolar) affinity for K^+, the Q116R mutation at the mouth of the SF lowers this affinity by three orders of magnitude and has been used historically for comparison between K^+-bound and K^+-free states (5, 10). The S162A mutation prevents phosphorylation of this serine, recently shown to be a regulatory modification that inhibits KdpFABC (9), thus confounding previous studies of the reaction cycle. We expressed this mutant complex in *Escherichia coli* and purified it in n-decyl-β-D-maltoside detergent using affinity chromatography followed by size-exclusion

chromatography (*SI Appendix*, Fig. S1 *B* and *C*). The purified protein complex was characterized both with ATPase assays of the detergent-solubilized samples and with K^+ transport assays after reconstitution into lipid vesicles demonstrating that the protein not only had robust activity, but that ATPase activity was coupled to transport (*SI Appendix*, Fig. S1 *D* and *E*). For cryo-EM imaging, aliquots of the detergent-solubilized samples were mixed with various substrate analogs followed by rapid freezing of EM grids. Work on other P-type ATPases has identified a variety of substrate analogs that trap specific reaction intermediates (11). Accordingly, AMP-PCP was used to stabilize the E1 state that precedes formation of the covalent aspartyl phosphate (E1-P), and four phosphate analogs were used to trap different E2 substates. BeF_3 has been shown previously to trap the prehydrolysis E2-P state, AlF_4 the transition state E2-P, and MgF_4 the posthydrolysis E2·Pi state in other P-type ATPases (12). Orthovanadate is another phosphate analog with a long history of inhibiting P-type ATPases (13). ATPase assays confirmed the inhibitory capabilities of these various compounds (*SI Appendix*, Fig. S1*D*), though it should be noted that turnover conditions with the presence of ATP and its reaction products are not truly representative of the inhibitory complexes produced for cryo-EM. For all but one substrate analog (MgF_4), we prepared samples in the presence of either 100 mM K^+, which is well above the 7 mM K_M for this construct, or 100 mM Na^+, which does not stimulate ATPase activity (7).

A total of 14 independent density maps were produced from the various samples using conventional methods of single-particle cryo-EM. Each data set comprised between 150,000 to 450,000

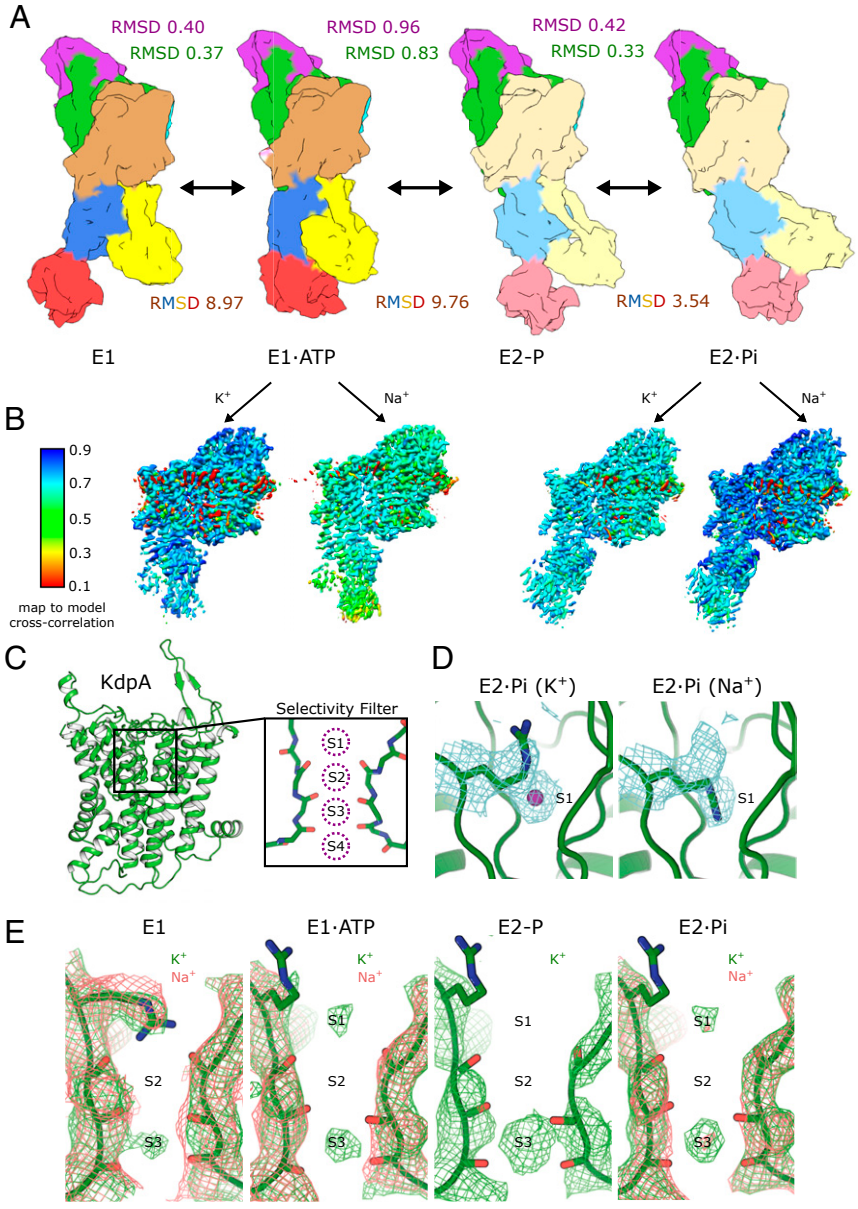

Fig. 2. Conformational changes accompany the reaction cycle. (*A*) Surface representations of the KdpFABC complex rendered at 10-Å resolution. rmsd values reflect comparison between individual subunits from adjacent conformational states (557, 672, and 186 Cα atoms for KdpA, KdpB, and KdpC, respectively). Text is colored according to the subunit being compared (see Fig. 1). (*B*) Map-to-model correlations showing little to no effect of K^+ binding. Atomic models were built for the map produced in the presence of K^+. (*C*) Illustration of the four binding sites for K^+ (S1 to S4) in the SF of KdpA. (*D*) Density at the S1 site in the E2·Pi state (contoured at 12σ) in the presence of either K^+ or Na^+. The bifurcated density suggests that Arg116 competes with K^+ at this site. (*E*) Densities within the SF in the presence of K^+ (green mesh) and Na^+ (red mesh). Contour levels are 10σ for E1, 11σ for E1·ATP, 17σ for E2-P, and 12σ for E2·Pi.

particles, and overall resolutions ranged between 2.9 and 3.7 Å. In two cases, different conformations were resolved from single datasets using three-dimensional classification. In the first case, samples treated with VO_4 produced structures of both E1 and E2 states, suggesting that this phosphate analog has relatively low affinity and binds to only a fraction of the molecules. In the second case, treatment with BeF_3 in the presence of K^+ also produced two distinct maps, but these appear to be pre- and posthydrolysis E2-P states, as is discussed in the next section, *Conformations of KdpB Confirm the Stabilization of Specific Reaction Intermediates*. From the 14 density maps, we chose the highest-resolution examples of the four unique conformational states that were observed, which were then used for model building and further detailed analysis. In addition, a second structure for the E2·Pi state was built for a direct comparison of structures in the presence of either K^+ or Na^+ (*SI Appendix*, Figs. S2–S5 and Table S1). Note that Na^+ was included in conditions lacking K^+ such that any differences reflect a specific binding of K^+ relative to Na^+.

Density maps representing the four main states in the reaction cycle are shown in Fig. 1 together with close-up views of the catalytic site of KdpB, where the substrate analogs bind. In the absence of substrates at the catalytic site (apo state), the A- and N-domains of KdpB are quite disordered, reflecting the innate mobility of these domains, which is explicitly depicted by an analysis of variability in the dataset (Movies S1–S3). Binding of ATP or phosphate analogs to the catalytic site stabilizes interactions between these domains and the P-domain, which carries the catalytic aspartate (Asp307). Densities for the analogs are clearly visible together with the key coordinating residues, except for those in the E2-P map, which had lower resolution in this region. Overall, KdpA, KdpC, KdpF, and the membrane domain of KdpB are well ordered, with clear visibility of side-chain density.

Conformations of KdpB Confirm the Stabilization of Specific Reaction Intermediates. The reaction intermediate represented by each structure was confirmed by comparing KdpB with SERCA. After alignment of P-domains, N- and A-domain placements are consistent with specific states of SERCA (*SI Appendix*, Fig. S6*A*). The E1 states show unliganded catalytic aspartic acids (Asp307 in KdpB and Asp351 in SERCA) that do not interact with either A- or N-domains, allowing them to retain their innate flexibility. The E1·ATP states show AMP-PCP molecules bound in equivalent pockets of the N-domains with the γ-phosphate poised for phosphoryl transfer; conserved residues coordinate the Mg^{2+} and the ATP analog in an analogous fashion, and the A-domain is displaced from the catalytic site (*SI Appendix*, Fig. S6*B*). It is notable that the A-domain adopts a different angle in the E1·ATP state: the conserved TGES loop is rotated clockwise from the catalytic site in KdpB, whereas this loop is rotated counterclockwise in SERCA as viewed from the cytoplasm. The prehydrolysis (E2-P) and posthydrolysis (E2·Pi) E2 states in both SERCA and KdpB have rather similar configurations at the catalytic site with the conserved TGES motif engaging the catalytic aspartate and displacing the N-domain. Although these two E2 states are difficult to distinguish solely on catalytic site residues, comparison of the linkage between cytoplasmic and membrane domains proves decisive. Specifically, the cytoplasmic extension of M2 becomes unwound in the transition between the E2-P and E2·Pi state of SERCA, producing a large-scale structural difference that affects the position of cytoplasmic domains relative the membrane domain (*SI Appendix*, Fig. S6*C*). KdpB undergoes an analogous change in which M2 is continuous through Lys98 in E2-P but becomes unwound after Leu85 in E2·Pi. As a result, the cytoplasmic domains move in a similar way, and the TGES loop is repositioned to reflect its role in hydrolysis of the aspartyl phosphate. These comparisons confirm that similar chemistry is at play in the reaction cycles of these two homologs and that substrate analogs stabilize KdpFABC in comparable enzymatic states from the Post–Albers cycle.

KdpA, KdpC, and KdpF and Structural Effects of K^+. In contrast to the large-scale conformational changes in KdpB, the other subunits of the complex are essentially unchanged as the molecule transitions between the different enzymatic states. Pairwise alignment of KdpA and KdpC produces rmsd values below 0.5 Å for C-α atoms, which reflects virtually no changes in the core structure and only slight changes in the peripheral loops of these subunits (Fig. 2*A*). These subunits are also unchanged compared to the crystal structure (rmsd values < 1.0), indicating that they remain rigid throughout the reaction cycle. In the E1 states, a salt-bridge network exists between cytoplasmic loops on KdpA (Arg400 and Ser517) and KdpB (Asp300 and Asp302, *SI Appendix*, Fig. S7*A*). According to our previous mechanistic model based on the crystal structure, these interactions play a role in energy coupling by pulling on a coupling helix ($D3M_2$ colored pink in *SI Appendix*, Fig. S7*A*) and opening a gate below the SF in KdpA (7). In order to test this model, we introduced the D300A/D302A mutation into the wild-type gene for kdpB and evaluated ATPase and transport activities after reconstitution of the purified complex into liposomes (*SI Appendix*, Fig. S7). If the model was correct, this double mutant would abolish coupling. However the results show that both constructs remain coupled, with robust transport activity, although the mutations reduce maximal activity by 20 to 30%. For the transport assay, we also evaluated ATP dependence, thus deducing K_M of 5.7 and 13.9 μM for wild-type and mutant protein, respectively. Given the modest effects of the D300A/D302A mutation, we conclude that this salt-bridge network is not likely to be crucial for the transport mechanism, suggesting that an alternative transport mechanism is likely.

Enzymatic activity of KdpFABC depends on the presence of the transport substrate K^+ with a K_M of 7 mM for the Q116R mutant (9). We therefore compared density maps from samples in the presence of either 100 mM K^+ or 100 mM Na^+ to look for K-dependent conformational changes. However, models created for the various states in the presence of K^+ correlate equally well with density maps for those same states produced in the presence of Na^+ (Fig. 2*B* and *SI Appendix*, Fig. S8). The only observed changes involve specific spherical densities within the SF of KdpA, which is characterized by four canonical sites: S1 to S4 (Fig. 2*C*) (14). At the S3 site, we consistently see a strong spherical density in maps derived from samples containing K^+ (Fig. 2*E*). This density was also seen in the crystal structure, and anomalous scattering was used to confirm its assignment as K^+ (7). When K^+ is absent, the S3 site density is much weaker or completely missing in our cryo-EM maps. We also observe density at the S1 site, which was occupied by the guanidino group of Arg116 in the crystal structure. As discussed, the Q116R mutation lowers the apparent K^+ affinity (increases K_M from micromolar to millimolar), and we previously hypothesized that this effect results from a competition between arginine and K^+ at this site (7). In support of this idea, some of our maps show bifurcated or ambiguous density for the Arg116 side chain, which can be modeled either inserted into the S1 site (e.g., E1) or residing just above it with a K^+ occupying the S1 site (e.g., E2·Pi with K^+, Fig. 2*D*). More global effects of the Q116R mutant can be ruled out by comparing our structures with earlier work using the wild-type protein (8) in which comparable conformations for the E1 and E2 states were observed with rmsd ~0.6 Å for KdpA.

Dimensions of the Transmembrane Tunnel. The intramembrane tunnel linking KdpA and KdpB is a unique feature of KdpFABC that we previously hypothesized to play a key role in the transport process. To look for changes during the reaction cycle, we plotted radii of the tunnel in the three highest-resolution structures (E1, E1·ATP, and E2·Pi) starting at the S1 site at entrance to the SF and traversing through this filter, across KdpA and into the Bx site in KdpB (Fig. 3). These plots illustrate the severe constriction of the SF, due to close apposition of carbonyl atoms that serve to distinguish

K^+ from other ions. Once past the SF, the intramembrane tunnel widens into a relatively spacious vestibule that extends about halfway to the KdpA–KdpB interface. Comparison of the various structures shows little change in the KdpA region of the tunnel, consistent with the observed rigidity of this subunit. In the E1 structures, the tunnel narrows to ∼1.4 Å as it approaches the subunit interface before widening again in the vicinity of the Bx site. In the E2·Pi structure, movements of M3 to M5 in KdpB introduce a bottleneck of ∼0.8 Å and also collapse the cavity next to Bx. Given the sensitivity of this analysis to accurate side-chain placements, the lower resolution of KdpB in the E2-P state (4 to 5 Å) reduces our confidence in the dimension of the tunnel in this region, but we have included the corresponding plot in Fig. 3*B* (dotted blue line) and *SI Appendix*, Fig. S9*C* for completeness.

The continuity of the intramembrane tunnel is influenced by a lipid molecule that we modeled at the interface of KdpA and KdpB. The lipid was placed into an elongated density that we observe in all of our density maps (*SI Appendix*, Fig. S9) and that was also observed in previously published cryo-EM maps (8). Tentative assignment of lipid is consistent with the bifurcated density visible in our best maps, which was further supported by mass spectrometry of the detergent-solubilized, purified complex used for our cryo-EM experiments (*SI Appendix*, Fig. S10). As expected from *E. coli*, phosphatidylethanolamine (PE) and phosphatidylglycerol (PG) with chain lengths of 16 or 18 carbons dominated the mass spectrum. The 16/18 species was most consistent with the densities in the maps (*SI Appendix*, Fig. S9*B*), and we therefore modeled a 16:0/18:1 PE molecule at the interface between M10 of KdpA and M7 of KdpB. This region changes during the E1 to E2 transition, during which M5 from KdpB moves away from the subunit interface, and one of the lipid tails is drawn in to fill the resulting space. As a result, the lipid molecule constricts the tunnel in the E2 states, though it does not affect tunnel radius in the E1 states (*SI Appendix*, Fig. S9*C*). In the absence of this lipid molecule, the intramembrane tunnel would be exposed to the hydrophobic core of the bilayer at the subunit interface, indicating that it plays an important structural role in the complex.

Character of the Intramembrane Tunnel of KdpA. The intramembrane tunnel was previously postulated to be either a water-filled cavity for charge transfer or a conduit for K^+ to move between the subunits (7, 8). We observe several well-defined densities in the tunnels in our density maps allowing us to evaluate these alternative scenarios. Specifically, comparison of our higher-resolution maps led to definition of seven distinct sites in KdpA (A1 to A7, Fig. 3*D* and *SI Appendix*, Fig. S11) in addition to two additional sites in KdpB (B1 and B2, Fig. 4). In KdpA, several of the densities are visible in all maps, but as expected, discrete sites are more easily identified in higher-resolution maps (*SI Appendix*, Fig. S11). Interestingly, the location and spacing of these densities is somewhat consistent from map to map, regardless of conformational state or presence of K^+. This result suggests that the tunnel is filled with a loosely ordered array of water molecules at all stages of the reaction cycle, and the densities have been modeled as such. At the bottom of the SF, the tunnel is fairly hydrophilic due to oxygen ligands from side chains of Asn112, Thr230, Ser343, and Asn466. Together with main-chain carbonyls from the SF, these side chains have potential to constitute the S4 site described in classical K^+ channels (Fig. 2*C*) (14). However, S4 is not well formed in KdpA or in its homologs TrkH and KtrB, and no density is observed here. The first two densities (A1 and A2) are seen as the tunnel extends away from the SF and widens into a vestibule with radius >2 Å, with side-chain oxygens from Ser343, Glu370, Ser378, Tyr381, Thr424, and Asn466 and the main-chain carbonyl of Ile421 producing a somewhat hydrophilic environment. Interactions of these residues and water molecules placed in the model are listed in *SI Appendix*, Table S2. Variability in the location and coordination of the water molecules together with a lack of organized coordination geometry suggest that they are only loosely bound. This situation is more consistent with a hydrated environment that facilitates movement of K^+ between the subunits rather than the water wire that was previously postulated to support charge transfer. As the tunnel approaches A7, it narrows and becomes distinctly hydrophobic, being lined by side chains from Phe386, Leu389, Ile421, and Val538 from KdpA as well as Ala-227 and Leu228 from KdpB. The A7 site is at the subunit interface and thus very near the end of an aliphatic tail from the lipid molecule discussed above in the section *Dimensions of the Transmembrane Tunnel*; the main-chain oxygen of I421 is the only plausible protein ligand near this site at a distance of 3.7 Å. Finally, the tunnel passes hydrophobic side chains on M2 and M5 of KdpB to reach the cavity near Pro264 and the Bx binding site seen in the crystal structure.

Spherical Densities in KdpB. In the crystal structure, the Bx site in KdpB is defined by the unwinding of M4 near Pro264 (Fig. 4*E*) and, here, a water is coordinated by backbone carbonyls of Val260 and Ile263 (M4) and by side chains of Thr265 (M4) and Asn624 (M6). This site is isosteric with the Ca(II) site seen in SERCA (15) and the Na(II) site in Na,K-ATPase (16, 17). Our E1 and E1·ATP maps of KdpFABC both display a discrete density in a nearby pocket between M4, M5, and M6, which we have modeled as water in a site we label B1 (Fig. 4). The B1 site is displaced toward M5, relative to Bx, and is close to the Ca(I) and Na(I) sites seen in SERCA and Na,K-ATPase (*SI Appendix*, Fig. S12). In our model for E1·ATP, water at the B1 site is coordinated by backbone carbonyls of Cys261 and Ile263 (M4), by the side chain of Asp583 (M5), and by a second water (B1' auxiliary site) that is coordinated by Thr266 (M4), Asn582, and Lys586 (M5). This extensive coordination network suggests that the B1 site could have relatively high affinity toward K^+. Indeed, the K(I) site in Na,K-ATPase is coordinated in a similar way by some of these same residues. Although there is access to the tunnel, the B1 site is otherwise occluded within the membrane domain of KdpB.

The configuration of this region of KdpB undergoes substantial changes in the E2 structures. In E2·Pi, where the resolution is high enough (2.9 Å) for accurate model building, no densities are seen in B1 or its ancillary B1' site. Indeed, this pocket has collapsed due to a downward movement of M5 that moves the amino group of Lys586 into the B1 site (Fig. 4). Instead, a spherical density is seen 9 Å away in a site between M2, M4, and M6. The density in this site, designated B2, has also been modeled as a water that interacts with the backbone carbonyl of Val260 and the amide nitrogen of Asn624; the less extensive coordination suggests that the affinity of this site for K^+ would be considerably lower than B1 and probably less selective. When Na^+ is substituted for K^+ in the buffer, it is likely that this site is occupied by Na^+, thus accounting for the density seen in the B2 site under these conditions (Fig. 4*D*). The B2 site is adjacent to a wide, water-filled cavity that opens toward the cytoplasm (*SI Appendix*, Fig. S13). This cavity was previously described by Stock et al. and proposed to be an exit site for ions in the E2 state (8). However, we see this cavity in all of our structures, including the crystal structure, and we are able to identify ordered water molecules occupying the cavity in higher-resolution structures of both E1·ATP and E2·Pi states (*SI Appendix*, Fig. S13).

Discussion

In this study, we have used substrate analogs to stabilize KdpFABC in different enzymatic states and have generated the corresponding structures using cryo-EM. Conformational changes seen in KdpB are consistent with four major intermediates in the Post–Albers reaction scheme, but a lack of changes in KdpA, KdpC, and KdpF suggest that they remain static during transport. As in previous work, an intramembrane tunnel is observed running from the SF in KdpA to the Bx site in KdpB. For the different reaction intermediates, the architecture of this tunnel is invariant within KdpA, whereas the tunnel undergoes substantial changes in KdpB during

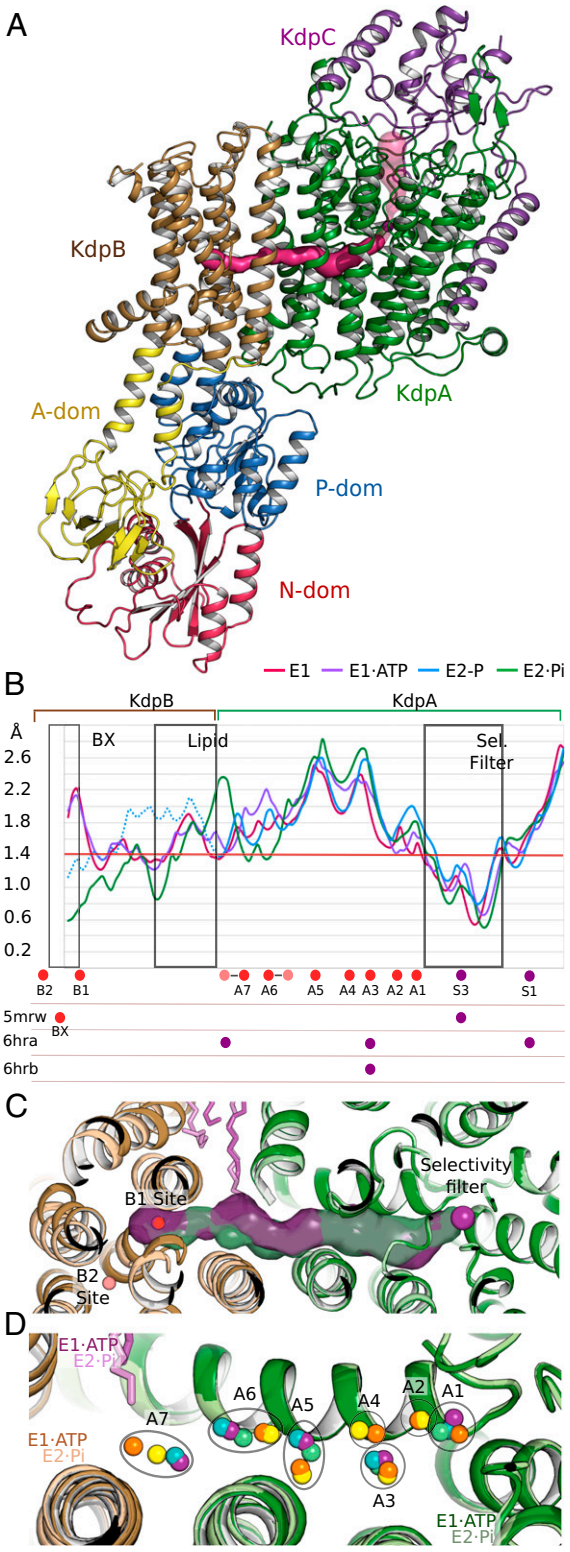

Fig. 3. Mapping of the intramembrane tunnel. (*A*) The intramembrane tunnel (pink) in the E1 state extends from the SF in KdpA to the B1 site in KdpB. (*B*) Tunnel radii in the four states as indicated in the legend. The E2-P state (dotted) is uncertain due to the lower resolution of this map; 1.4 Å corresponds to the conventional threshold for water and K^+. Locations of densities modeled as water (red) or K^+ (purple) in various maps are shown *Below*. (*C*) Tunnel surfaces from E1·ATP (purple) and E2·Pi (green) states; atomic models are also shown with E1·ATP rendered in darker colors. Purple sticks correspond to lipid molecules. (*D*) Densities within the intramembrane tunnel viewed from the periplasm with ribbon models for the E1·ATP (dark colors) and E2·Pi (light colors) states. Sphere are colored as follows: E1 (K^+): purple; E1·ATP (K^+): blue; E2-P (K^+): green; E2·Pi (Na^+): yellow; and E2·Pi (K^+), orange.

the transition from E1·ATP to E2·Pi. Although the tunnel is buried within the protein domains, it has constricted access both to the periplasm through the SF of KdpA and to the cytoplasm via a water-filled cavity in KdpB. Our density maps reveal discrete spherical densities in the SF, in the tunnel, and near the Bx site of KdpB; understanding the nature of these densities likely holds the key to understanding the mechanism of transport.

Assignment of the Spherical Densities. Although it is not possible to make definitive atomic assignments for densities in a cryo-EM map, the spherical densities in our maps most likely correspond either to water molecules, K^+, or Na^+ ions. Comparison of maps derived from structures in the presence of K^+ and Na^+ provide clues. Within the SF, a strong density is seen at the S3 site in samples containing K^+, and this density is either absent or considerably weaker when K^+ is absent, making assignment at this location straightforward, while highlighting the ability of both water and K^+ to bind in these sites (18). A second, more variable density is seen in the S1 site, which could be assigned either as K^+, water, or as the guanidinium group of Arg116 (Fig. 2). Density at the S1 site was also seen in the previous cryo-EM structure of the E1 state (8). The construct used in this earlier work carried the wild-type Gln116, supporting the idea that lower affinity produced by the Q116R mutation used here reflects competition for the S1 site ligands at the entrance to the SF. The lower coordination at S1 (five oxygen ligands) compared to S3 (eight oxygen ligands, *SI Appendix*, Table S2) suggests that S3 is the main determinant of K^+ selectivity, as discussed previously (7). Densities have so far not been observed in the S2 or S4 sites, which is consistent with the idea that KdpA is optimized for equilibrium binding of ions, in contrast to the non-equilibrium behavior utilized by channels that promotes rapid exchange between the sites (14). In the absence of K^+, either water or possibly Na^+ would be expected to bind within the SF to prevent collapse (19). Although Na^+ binding to the SF is theoretically possible, the strong selectivity of KdpFABC suggests that this ion would not be allowed to pass through the SF and enter into the tunnel.

In contrast to the SF, the map densities within the tunnel itself do not depend on the presence of K^+, making it likely that these represent water. The region near the SF is hydrophilic and becomes relatively wide (radius ~2.4 Å) in the vicinity of A3 to A6, raising the possibility that a K^+ ion could move past the water molecules and enter the more hydrophobic and constricted region near the KdpA/KdpB interface (radius ~1.4 Å). Although there are some polar moieties available to coordinate atoms in the tunnel (*SI Appendix*, Table S2), they do not constitute an organized binding site, such as seen in the SF. Thus, equilibrium binding by K^+ in this region is unlikely.

In KdpB, spherical densities are also observed in the presence of either K^+ or Na^+, but their locations depend on the enzymatic state. In the maps of the E1·ATP state, two densities are observed at the B1 site in K^+ buffer, but only one density is seen in Na^+ buffer. This observation suggests that the density at the B1 site corresponds to K^+, and the nearby density (B1') is a water molecule that helps to coordinate the ion when it is present. Water molecules are similarly seen in SERCA and Na,K-ATPase coordinating their transport substrates (*SI Appendix*, Fig. S12). As in these other P-type ATPases, the B1 site in KdpFABC is well coordinated with four surrounding ligands (*SI Appendix*, Table S2) suggesting that it is a high-affinity site. In the E2·Pi state, the B2 site is occupied in the presence of either K^+ or Na^+. The B2 site is coordinated by only two side chains which indicate that B2 corresponds to a low-affinity, nonselective release site, which could be occupied by K^+, Na^+, or water.

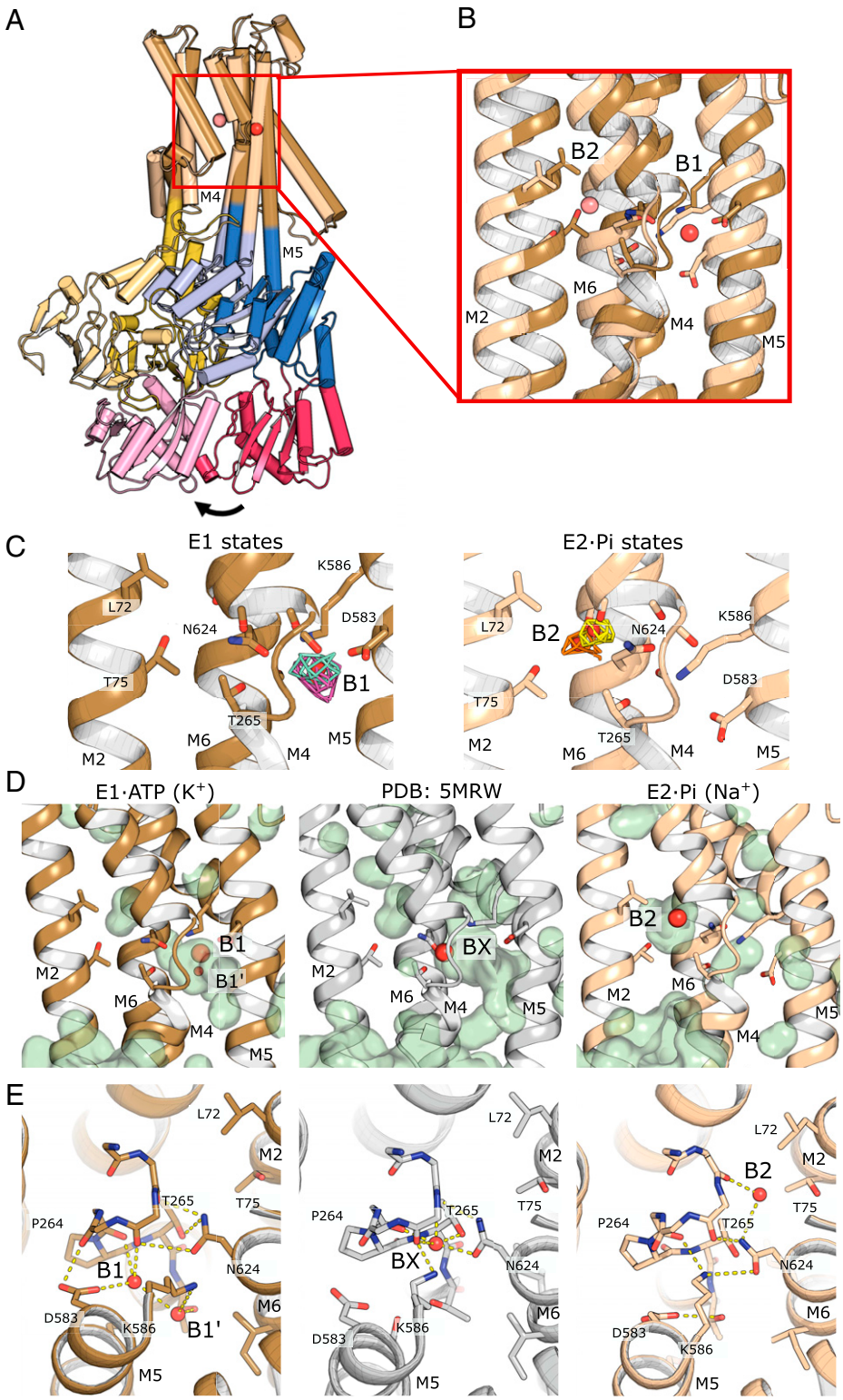

Fig. 4. Alternate binding pockets in KdpB. (*A*) KdpB in E1·ATP and E2·Pi states illustrating large movements of cytoplasmic domains and M5. E1·ATP is rendered in darker colors. Structures were aligned on KdpA. (*B*) Close-up of B1 and B2 sites showing displacement of K586 into the B1 site in E2·Pi. (*C*) Experimental density in B1 and B2 sites contoured at 6σ: E1 [K^+], purple; E1·ATP [K^+], cyan; E2·Pi [K^+], yellow; and E2·Pi [Na^+], orange. (*D*) Cavities observed in different states (pale green) determined with a solvent radius of 1.4 Å. (*E*) Coordination at the various sites viewed from the periplasm.

Comparison with Other P-Type ATPases. Structures both from the current work and from previous work (7, 8) indicate that KdpA is a static element that serves to select K^+ from the periplasm and load the transport site of KdpB from within the transmembrane domain. KdpB then functions as an ion pump, like other members of the P-type ATPase superfamily. Thus, comparison of ion binding sites in KdpB, SERCA, and Na,K-ATPase sheds light on the mechanism of transport (*SI Appendix*, Fig. S12). Both of these

other pumps bind multiple cations with a net positive charge of 2 to 4. As a consequence, the overall neutral charge of the binding site in KdpB is replaced by multiple acidic residues in SERCA and Na,K-ATPase. In particular, Lys586 in KdpB is replaced by a glutamate, and additional aspartate and glutamate residues are present on M4, M6, and M8, all of which participate in ion coordination. From a mechanistic point of view, both SERCA and Na,K-ATPase are designed to release ions to the extracellular side of the membrane in E2-P, whereas KdpFABC releases ions to the cytoplasm. The release in SERCA and Na,K-ATPase is dependent on large movements of M4 and M6, which not only disrupt the coordination network for the ions but also open an exit pathway. In KdpB, the periplamic sides of the membrane helices do not change much between E1 and E2 states, suggesting that a single K^+ is simply passed from the B1 to the B2 site where there is a constitutive release pathway present in all of our structures. Despite these conformational differences, there are similarities in the architecture of the ion sites. The B1 site in KdpB, the Ca(I) site in SERCA, and the Na(I) site in Na,K-ATPase are all coordinated by homologous residues on M4 and M5 and ancillary water molecules. The Bx site in KdpB is very similar to the Ca(II) site in SERCA and the Na(II) site in Na,K-ATPase, with comparable coordination by main-chain carbonyls on M4 and by Asn624 on M6. Asn624 is conserved with Asn796 on SERCA and Asp800 on Na,K-ATPase; this residue defines a boundary to the ion sites in all three proteins. In SERCA and Na,K-ATPase, the transport ions remain on one side of this boundary, but in KdpB the ion is transferred to the B2 site on the other side of M4. This transfer appears to be the key, energy-dependent step for KdpFABC. The Bx site seen in the crystal structure is halfway between B1 and B2 sites and may therefore be intermediate in this process.

Structural Basis for K^+ Transport. Assignment of densities within the transmembrane domains and conformational changes in KdpB allow us to articulate the steps in the transport cycle (Fig. 5). To begin, ions move through the SF in a constitutive manner with selection of K^+ over other ions occurring at the S3 site. K^+ is allowed to transit the tunnel and reach the B1 site in E1 or E1·ATP states, given the uninterrupted nature of the tunnel in these states. In the B1 site of KdpB, K^+ is coordinated by Asp583 as well as two main-chain carbonyls from M4 and the nearby water molecule in site B1', which is itself coordinated by Lys586, Asn582, and Thr266. Asn624 on M6 plays an important role in demarcating this site and holding Lys586 in position. During transition to E2-P, K^+ is transferred to the B2 site on the other side of M4 and Asn624, a site with minimal coordination and presumably lower affinity. Although there is no cavity connecting the B1 and B2 sites in the structures, the Bx site offers an intermediate position that could mediate transfer. The Bx site is occupied in the crystal structure, which is thought to represent an inhibited state, due to phosphorylation of Ser162. Kinetic analyses indicated that phosphorylation of Ser162 trapped the complex in the E1-P state (9), which is an intermediate between the E1·ATP and E2-P states represented by our cryo-EM structures. Ion binding at the Bx site is therefore likely to mimic an occluded state associated with a true E1-P intermediate. The positively charged Lys586 plays a key role in the transition to the E2·Pi state as it swings over to occupy the B1 site due to movements in M5; these movements are instigated by the cytoplasmic domains, thereby representing a crucial energy-dependent step in the cycle. The movements also displace Asp583, which is returned to its coordination with Thr266. Both Asp583 and Lys586 were previously shown to be necessary for coupling ATPase activity and K^+ transport (20). Another consequence of M5 movement is a pinching of the tunnel at the interface between KdpA and KdpB, thus preventing K^+ from moving backward into the tunnel. Once the ion has been delivered to the B2 site in E2-P, it is close to a water-filled pathway leading to the cytoplasm between M1, M2, M3, and M4. Although there is a constriction in our models that would deny direct access of the B2 site to the cytoplasm, it is wider and shorter in the E2·Pi state (*SI Appendix*, Fig. S13). The constriction features hydrophilic residues Thr75 and Thr265, which could facilitate escape of the ion, and is lined by M1 and M2 helices. These helices have been shown in other P-type ATPases to move relative to the core membrane helices (21, 22), suggesting that this N-terminal region may have enhanced dynamics, especially because M1 is not tethered to the A-domain in KdpB. It should also be noted that this water-filled exit pathway is present in all observed conformations of KdpB, suggesting that the energy-dependent step is delivery of ions from B1, via Bx, to the low-affinity B2 site, after which they are readily released to the cytoplasm without further changes to the membrane domain.

Concluding Remarks

Cells across all kingdoms of life require high levels of intracellular K^+, but the transport systems responsible for homeostasis vary. Under normal conditions, K^+ transport in prokaryotes is handled by SKT and Kup transporters (23), as is also the case in plants (24), while animals use Na,K-ATPase (25). KdpFABC evolved to handle stress conditions, and its mechanism is unlike other P-type pumps: it borrows a channel-like subunit from the SKT superfamily to select the transport substrate, which is delivered within the membrane domain to the pump-like subunit from the P-type ATPase superfamily and then is moved into a preformed, secondary release cavity rather than relying on conformational changes to alter access to the primary, canonical binding site. This partnership

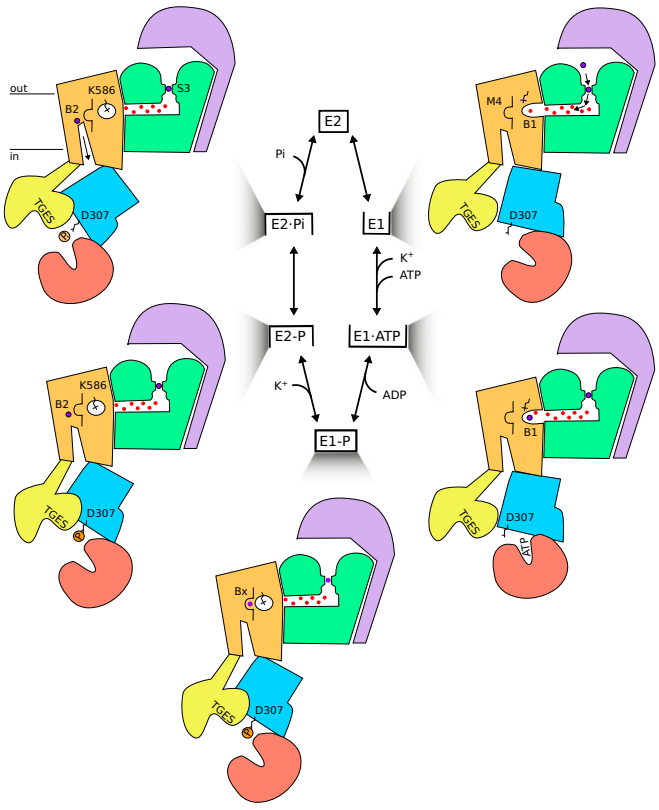

Fig. 5. Reaction mechanism of KdpFABC. K^+ enters the SF of KdpA (green) in the E1 state and travels through the water-filled tunnel to reach the B1 site in KdpB (brown). In the E1-P state, the ion moves to the Bx site, motivated by movement of Lys586 (shown as a crooked stick), and the intramembrane tunnel is pinched off at the subunit interface, thus generating an occluded state. Transition to the E2-P state moves the ion into the low-affinity B2 site on the other side of M4 (open loop). Hydrolysis of the aspartyl phosphate produces E2·Pi, thus facilitating release of K^+ via a preformed exit pathway to the cytoplasm.

appears to be stabilized by accessory subunits, KdpC and KdpF, as well as by a lipid molecule that fills a crucial gap at the subunit interface. Although our mechanistic model defines the basic steps in the reaction cycle, a number of important questions remain. What are the energetics of K^+ passing through the narrow, hydrophobic part of the tunnel and the transition between B1 and B2 sites? Is the stoichiometry one K^+ per ATP, and does transport of water accompany the transport of K^+? What are the determinants of the low-affinity B2 sites, and what are the energetics of release? Finally, what is the allosteric coupling that governs the inhibitory effects of Ser162 phosphorylation in the A-domain. The current work provides a framework to address these questions and to better appreciate the diverse roles of P-type ATPases in biology.

Methods

KdpFABC was expressed from a plasmid in *E. coli* using the endogenous promoter that responds to K^+ deficiency in the media. A construct carrying the KdpA-Q116R and KdpB-S162A mutations was used for all of the cryo-EM structures. Protein was purified by Ni-NTA affinity chromatography and then by size-exclusion chromatography in a buffer containing 25 mM Tris pH 7.5, 10% glycerol, 1 mM TCEP, 100 mM NaCl, and 0.15% n-decyl-β-maltoside. After addition of various substrates listed in *SI Appendix*, Table S1, samples were plunge frozen on Ultrafoil grids and imaged using a Titan Krios electron microscope (Thermo Fisher Scientific). Structures were determined using cryoSPARC (26) and atomic models were refined using PHENIX (27). Comparison of maps was performed using the EMDA program from the CCP-EM software suite (28, 29), and analysis of internal cavities was performed using Caver Analyst 2.0 Beta (30). ATPase activity of KdpFABC was assessed using a coupled enzyme assay (31), and electrogenic K^+ transport in reconstituted proteoliposomes (32) was monitored either with the voltage-sensitive dye $DisC_3$ or by capacitative coupling using the $SURFE^2N1$ (Nanion Technologies). Lipid content of the preparation was determined by liquid chromatography–mass spectrometry as previously described (33). Additional details of these procedures is provided in *SI Appendix*.

Data Availability. Atomic models have been deposited in the Protein Data Bank (PDB) and Cryo-EM maps have been deposited in the Electron Microscopy Data Bank (EMDB) (PDB ID: 7BH1 (E1 state with K^+), 7LC3 (E1-ATP state), 7LC6 (E2-P state), 7BH2 (E2·Pi state with BeF_3 and K^+), and 7BGY (E2·Pi state with MgF_4 and Na^+); EMDB ID: 12184–12186, 23268, 23269, 23342–23344, 23346–23349, 23353, and 23354). All study data are included in the main text or in the *SI Appendix*.

ACKNOWLEDGMENTS. Funding for this work was provided by NIH Grant No. 1R01GM108043 to D.L.S., Aarhus Institute for Advanced Studies with funding from the European Union's 2020 research and innovation programme under the Marie Sklodowska-Curie Grant Agreement No. 754513 and the Aarhus University Research Foundation to D.L.S., and by funding from the Independent Research Fund Denmark (Grant No. DFF-8021-00161) to B.P.P. Electron microscopy was performed at the Cryo-EM Core Facility at New York University Langone Health, with the assistance of William Rice and Bing Wang. In addition, electron microscopy was performed at the Pacific Northwest Center for Cryo-EM at Oregon Health Sciences University, which was supported by NIH Grant No. U24GM129547 and accessed through Environmental Molecular Sciences Laboratory (grid.436923.9), a Department of Energy, Office of Science User Facility sponsored by the Office of Biological and Environmental Research, and at the Simons Electron Microscopy Center located at the New York Structural Biology Center, supported by grants from the Simons Foundation (Grant No. SF349247) and New York State Division of Science, Technology and Innovation (NYSTAR).

1. K. Altendorf *et al*., Osmotic stress. *Ecosal Plus*, 10.1128/ecosalplus.5.4.5 (2009).
2. J. C. Greie, The KdpFABC complex from *Escherichia coli*: A chimeric K+ transporter merging ion pumps with ion channels. *Eur. J. Cell Biol.* **90**, 705–710 (2011).
3. E. T. Buurman, K. T. Kim, W. Epstein, Genetic evidence for two sequentially occupied K^+ binding sites in the Kdp transport ATPase. *J. Biol. Chem.* **270**, 6678–6685 (1995).
4. S. R. Durell, E. P. Bakker, H. R. Guy, Does the KdpA subunit from the high affinity K(+)-translocating P-type KDP-ATPase have a structure similar to that of K(+) channels? *Biophys. J.* **78**, 188–199 (2000).
5. A. Siebers, K. Altendorf, Characterization of the phosphorylated intermediate of the K^+-translocating Kdp-ATPase from Escherichia coli. *J. Biol. Chem.* **264**, 5831–5838 (1989).
6. B. P. Pedersen, D. L. Stokes, H. J. Apell, The KdpFABC complex - K^+ transport against all odds. *Mol. Membr. Biol.* **35**, 21–38 (2019).
7. C. S. Huang, B. P. Pedersen, D. L. Stokes, Crystal structure of the potassium-importing KdpFABC membrane complex. *Nature* **546**, 681–685 (2017).
8. C. Stock *et al*., Cryo-EM structures of KdpFABC suggest a K^+ transport mechanism via two inter-subunit half-channels. *Nat. Commun.* **9**, 4971 (2018).
9. M. E. Sweet *et al*., Serine phosphorylation regulates the P-type potassium pump KdpFABC. *eLife* **9**, 9 (2020).
10. W. Epstein, V. Whitelaw, J. Hesse, A K+ transport ATPase in *Escherichia coli*. *J. Biol. Chem.* **253**, 6666–6668 (1978).
11. J. V. Møller, C. Olesen, A. M. Winther, P. Nissen, The sarcoplasmic Ca^{2+}-ATPase: Design of a perfect chemi-osmotic pump. *Q. Rev. Biophys.* **43**, 501–566 (2010).
12. S. J. Danko, H. Suzuki, The use of metal fluoride compounds as phosphate analogs for understanding the structural mechanism in P-type ATPases. *Methods Mol. Biol.* **1377**, 195–209 (2016).
13. P. L. Pedersen, E. Carafoli, Ion motive ATPases. 1. Ubiquity, properties, and significance to cell function. *Trends in Biological Sciences* **12**, 146–150 (1987).
14. S. Liu, S. W. Lockless, Equilibrium selectivity alone does not create K+-selective ion conduction in K+ channels. *Nat. Commun.* **4**, 2746 (2013).
15. C. Toyoshima, M. Nakasako, H. Nomura, H. Ogawa, Crystal structure of the calcium pump of sarcoplasmic reticulum at 2.6 A resolution. *Nature* **405**, 647–655 (2000).
16. M. Nyblom *et al*., Crystal structure of Na+, K(+)-ATPase in the Na(+)-bound state. *Science* **342**, 123–127 (2013).
17. R. Kanai, H. Ogawa, B. Vilsen, F. Cornelius, C. Toyoshima, Crystal structure of a Na+-bound Na+,K+-ATPase preceding the E1P state. *Nature* **502**, 201–206 (2013).
18. Y. Zhou, R. MacKinnon, The occupancy of ions in the K+ selectivity filter: Charge balance and coupling of ion binding to a protein conformational change underlie high conduction rates. *J. Mol. Biol.* **333**, 965–975 (2003).
19. M. O. Jensen *et al*., Mechanism of voltage gating in potassium channels. *Science* **336**, 229–233 (2012).
20. M. Bramkamp, K. Altendorf, Single amino acid substitution in the putative transmembrane helix V in KdpB of the KdpFABC complex of *Escherichia coli* uncouples ATPase activity and ion transport. *Biochemistry* **44**, 8260–8266 (2005).
21. M. Hiraizumi, K. Yamashita, T. Nishizawa, O. Nureki, Cryo-EM structures capture the transport cycle of the P4-ATPase flippase. *Science* **365**, 1149–1155 (2019).
22. T. L. Sørensen, J. V. Møller, P. Nissen, Phosphoryl transfer and calcium ion occlusion in the calcium pump. *Science* **304**, 1672–1675 (2004).
23. W. Epstein, The roles and regulation of potassium in bacteria. *Prog. Nucleic Acid Res. Mol. Biol.* **75**, 293–320 (2003).
24. I. Dreyer, N. Uozumi, Potassium channels in plant cells. *FEBS J.* **278**, 4293–4303 (2011).
25. M. V. Clausen, F. Hilbers, H. Poulsen, The structure and function of the Na,K-ATPase isoforms in health and disease. *Front. Physiol.* **8**, 371 (2017).
26. A. Punjani, J. L. Rubinstein, D. J. Fleet, M. A. Brubaker, cryoSPARC: Algorithms for rapid unsupervised cryo-EM structure determination. *Nat. Methods* **14**, 290–296 (2017).
27. P. D. Adams *et al*., PHENIX: A comprehensive Python-based system for macromolecular structure solution. *Acta Crystallogr. D Biol. Crystallogr.* **66**, 213–221 (2010).
28. C. Wood *et al*., Collaborative computational project for electron cryo-microscopy. *Acta Crystallogr. D Biol. Crystallogr.* **71**, 123–126 (2015).
29. T. Burnley, C. M. Palmer, M. Winn, Recent developments in the CCP-EM software suite. *Acta Crystallogr. D Struct. Biol.* **73**, 469–477 (2017).
30. A. Jurcik *et al*., CAVER Analyst 2.0: Analysis and visualization of channels and tunnels in protein structures and molecular dynamics trajectories. *Bioinformatics* **34**, 3586–3588 (2018).
31. G. B. Warren, P. A. Toon, N. J. Birdsall, A. G. Lee, J. C. Metcalfe, Reconstitution of a calcium pump using defined membrane components. *Proc. Natl. Acad. Sci. U.S.A.* **71**, 622–626 (1974).
32. K. Fendler, S. Dröse, K. Altendorf, E. Bamberg, Electrogenic K^+ transport by the Kdp-ATPase of *Escherichia coli*. *Biochemistry* **35**, 8009–8017 (1996).
33. M. Schlame, Y. Xu, H. Erdjument-Bromage, T. A. Neubert, M. Ren, Lipidome-wide ^{13}C flux analysis: A novel tool to estimate the turnover of lipids in organisms and cultures. *J. Lipid Res.* **61**, 95–104 (2020).